Supplementary Information (SI) for Environmental Science: Nano.
This journal is © The Royal Society of Chemistry 2026

Supplementary Information

Trace Level Arsenic(III) Ion Detection in Water with Liquid-Gated rGO/GO Field Effect Transistor Based Sensor

Arijit Pattra, Bathula Satwik, Himanshu Pramod Padole and Sayan Dey*

S1. Synthesis of Graphene Oxide (GO) nano flakes

0.5 g of graphite powder (flake size under 20 µm) and 0.5 g of sodium nitrate were introduced to 25 mL of (H_2SO_4) and stirred continuously for 30 minutes in an ice bath in order to maintain the temperature below 5°C. Then, 3 grams of ($KMnO_4$) were gradually introduced under continuous stirring for almost two hours, maintaining the temperature remained below 5°C. The resulting solution was thereafter placed in a water bath at 40°C and agitated for 2 hours until its colour transformed to a blackish brown. 50 ml of deionized water was thereafter added and stirred for one hour at 95°C. Subsequently, an additional 100 ml of deionized water was incorporated and agitated for an additional 30 minutes. Following that, 3 mL of a 30% v/v (H_2O_2) solution was introduced, resulting in a rapid colour transition from dark brown to bright yellow. Excess acid was eliminated using vacuum filtration with cellulose filter paper, and the precipitate was collected and suspended in 500 mL of deionized water. A series of centrifugations at 4500 rpm for 10 minutes was conducted, and the supernatant was removed until the precipitate dispersion attained a pH of 7. Ultimately, any un-exfoliated graphite was eliminated using centrifugation at 1000 rpm for 2 minutes, repeated two to three times, and the supernatant was collected. Multiple centrifugations at different optimized speeds, each lasting 15 minutes, were conducted to get flakes of varying diameters. The optimized speed of 7000 rpm was established and consistently maintained for all samples in this experiment.

S2. Substrate Preparation

A p-type <100> Si wafer was taken in this process. To effectively remove the impurities from the wafer's surface, RCA cleaning technique was employed. Initially, the Si wafer was washed with a mixture of 1:1 by volume of sulfuric acid (H_2SO_4) and hydrogen peroxide (H_2O_2). This mixture was prepared carefully by drop-wise adding of H_2O_2 in H_2SO_4 due to high exothermic nature of the reaction. Further, the substrate was dipped in a solution of 1% buffered HF solution to remove the native oxide from the Si surface. Following this step, the wafer was dried and placed in the furnace where thermal oxidation was performed at 1050°C for a duration of four hours. After the oxidation process, the wafer was then cooled naturally and the oxidized wafer was considered for further fabrication process.

S3. Atomic Force Microscopy (AFM) of the receptor layer (GO)

AFM performed on GO showed the uniformity of the thickness of the layer and the thickness was found to be around 600 nm as shown in fig. S1.

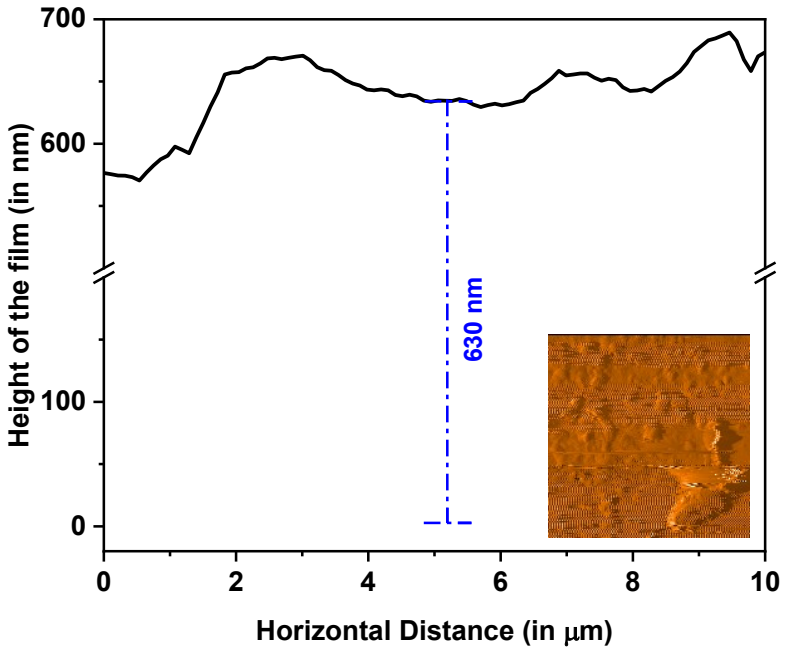

Figure S1. AFM image of the receptor layer (GO) showing the thickness of the layer deposited on top of the semiconductor layer

S4. Compositional Characterization

Compositional characterization carried out using Raman and XPS techniques. Successful reduction of GO to get reduced graphene oxide (rGO) is successfully verified using Raman spectroscopy as shown in fig. S2 b) and (c). The D and G bands for rGO was found at 1360 cm^{-1} and 1585 cm^{-1} which was found to be shifted after the reduction of GO which was 1364 cm^{-1} and 1580 cm^{-1}. The I_D/I_G for GO was found to be 1.48 which increased to 2.09 for rGO due to reduction in the oxygen functionalities compared to GO. rGO was further investigated using X-ray photoelectron spectroscopy (XPS). The deconvoluted XPS spectrum of C 1s peaks and O 1s peaks with binding energies of 284.25 eV, 285.71 eV and 287.98 eV correspond to C-C , C-OH and O-C=O bonds respectively for GO and 284.07 eV, 285.74 eV and 287.93 eV corresponds to C-C , C-OH and C=O bonds for rGO respectively. C/O peak ratio for GO was found to be 1.75 which increased to 2.65 for rGO. The presence of O=C–OH mainly responsible for the sensing of As(III) ions in water.

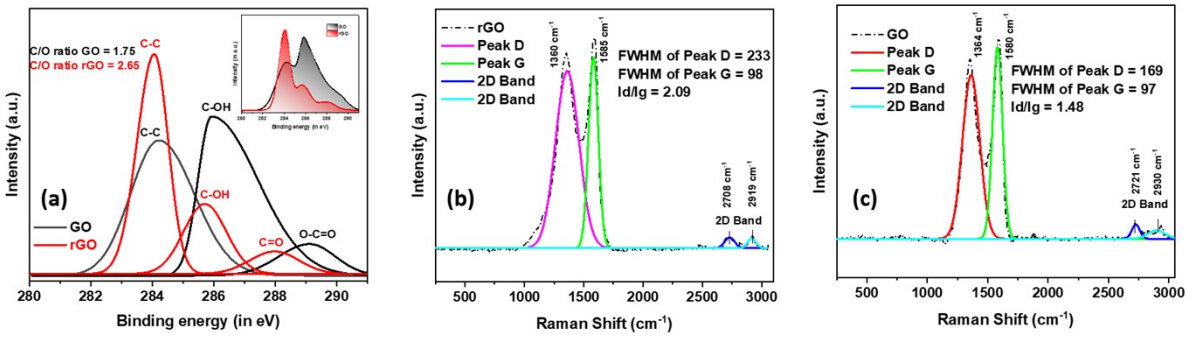

Figure S2. Structural and morphological characterization (a) X-ray photoelectron spectroscopy (XPS) of rGO (b) Raman spectra for rGO (c) Raman spectra for GO

S5. Fourier Transform Infrared spectroscopy (FTIR) of GO in absence and presence of As(III) ions

FTIR of the receptor layer (GO) was performed both in absence and presence of As(III) ions. A slight shift in the peak of the carboxyl group is observed in presence of As(III) ions marking the interaction of the ions with carboxyl (-COOH) group as shown in fig. S3.

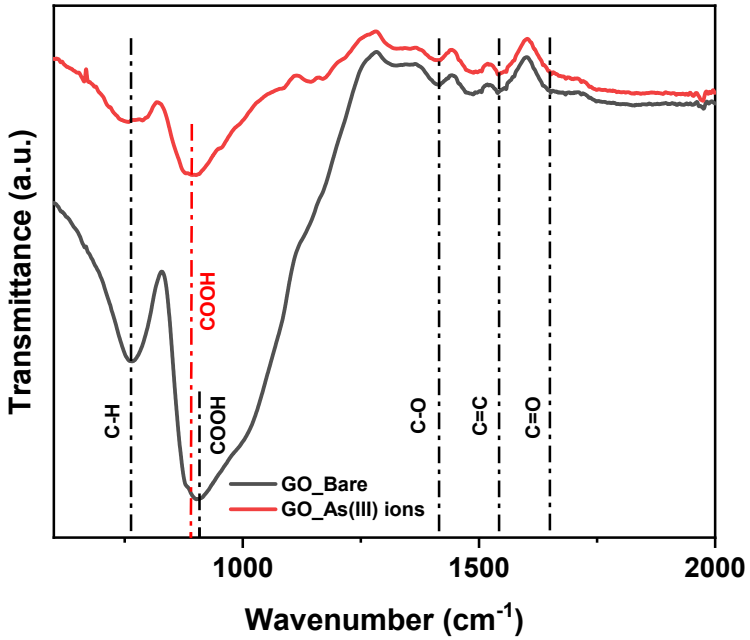

Figure S3. FTIR spectrum of the receptor layer (GO) in absence and presence of As(III) ions

S6. I-V characteristics of all rGO Ion-Sensitive Field Effect Transistors (ISFET)

This characteristics of the Field Effect Transistor (FET) describe how the drain current I_D varies with the drain-to-source voltage V_{DS}. As rGO is a p-type semiconductor, V_{DS} is varied from 0V to -10V and corresponding the value of I_D is plotted. V_{GS} is varied from 0V to -4V with an increment of 0.5V as shown in fig. S4. Device exhibits a threshold voltage of approximately 0.3 V, with a conductive channel forming when the gate voltage V_{GS} exceeds this threshold. As V_{DS} is increased, the device is observed to go into saturation which infers the channel formed in between drain and source moves towards the pinch-off condition and hence a saturation region is observed for every gate voltage as shown in fig. S4.

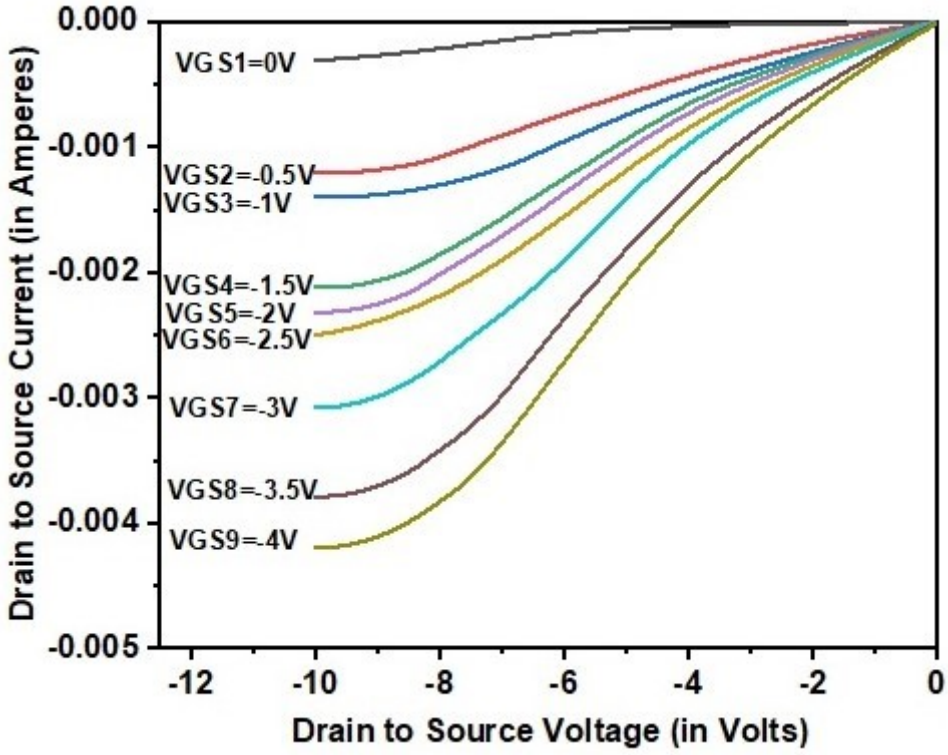

Figure S4. Current vs Voltage characteristics of the device with the increase in gate voltage

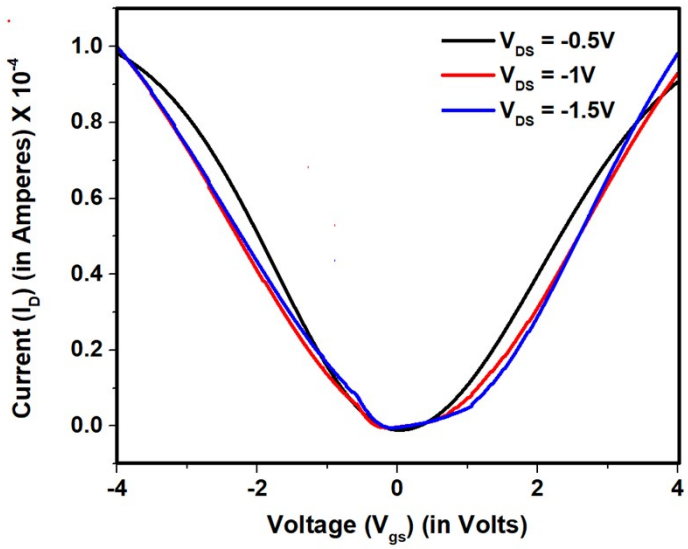

Figure S5. Current vs Voltage characteristics of the device with the increase in drain voltage

This characteristics of the FET describes how the drain current I_D varies with the gate-to-source voltage $V_{GS.}$ The V_{GS} is varied from -4V to 4V and corresponding the value of the drain current is plotted. V_{DS} is varied from 0V to -1.5V with an increment of 0.5V as shown in fig. S5. The plot represents the ambipolar nature of the device i.e., both hole conduction as well as electron conduction in the device is observed. As the drain to source voltage is increased the V-shaped plot moves towards the right side representing the semiconductor (rGO) is tending to become more p-type. On/off ratio of the device is found to be 8 and transconductance is found to be 17.7 µA/V.

S7. Box whisker plot for different concentrations of As(III) ions

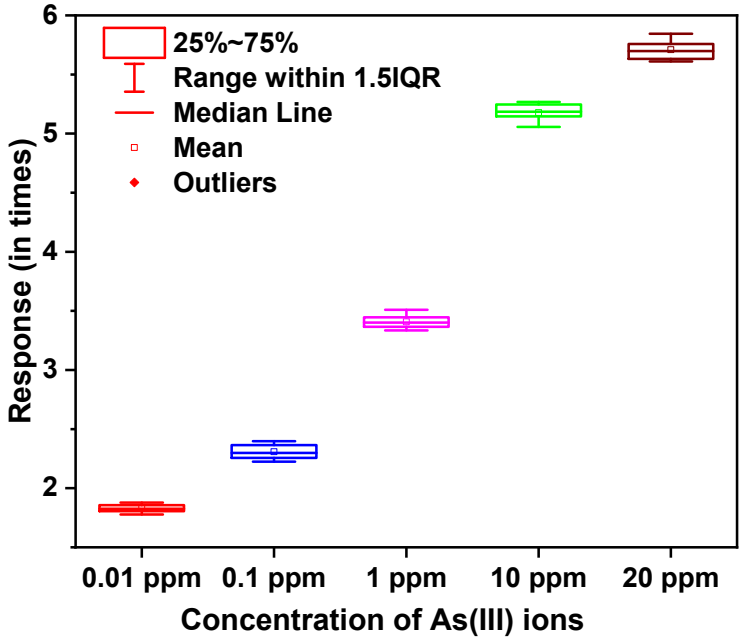

Figure S6. Box whisker plot of the sensing FET based device at 0.01 ppm, 0.1 ppm, 1 ppm, 10 ppm and 20 ppm of As(III) ions

S8. Box whisker plot for different ions at 1 ppm

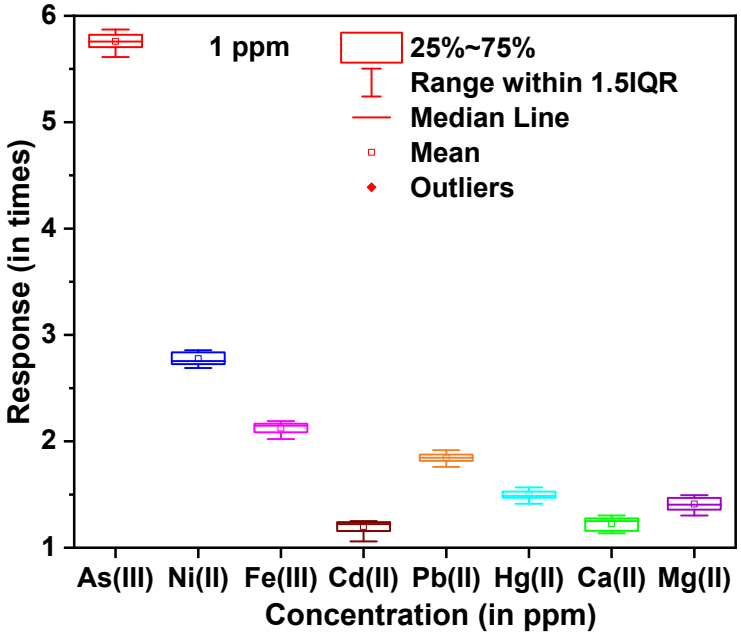

Figure S7. Box whisker plot of rGO/GO FET based device for different ions at 40 ppm concentration

S9. 3-sigma separation plot for the response of the FET based device towards different concentration of As(III) ions and response of the device towards different heavy metal ions at 40 ppm concentration

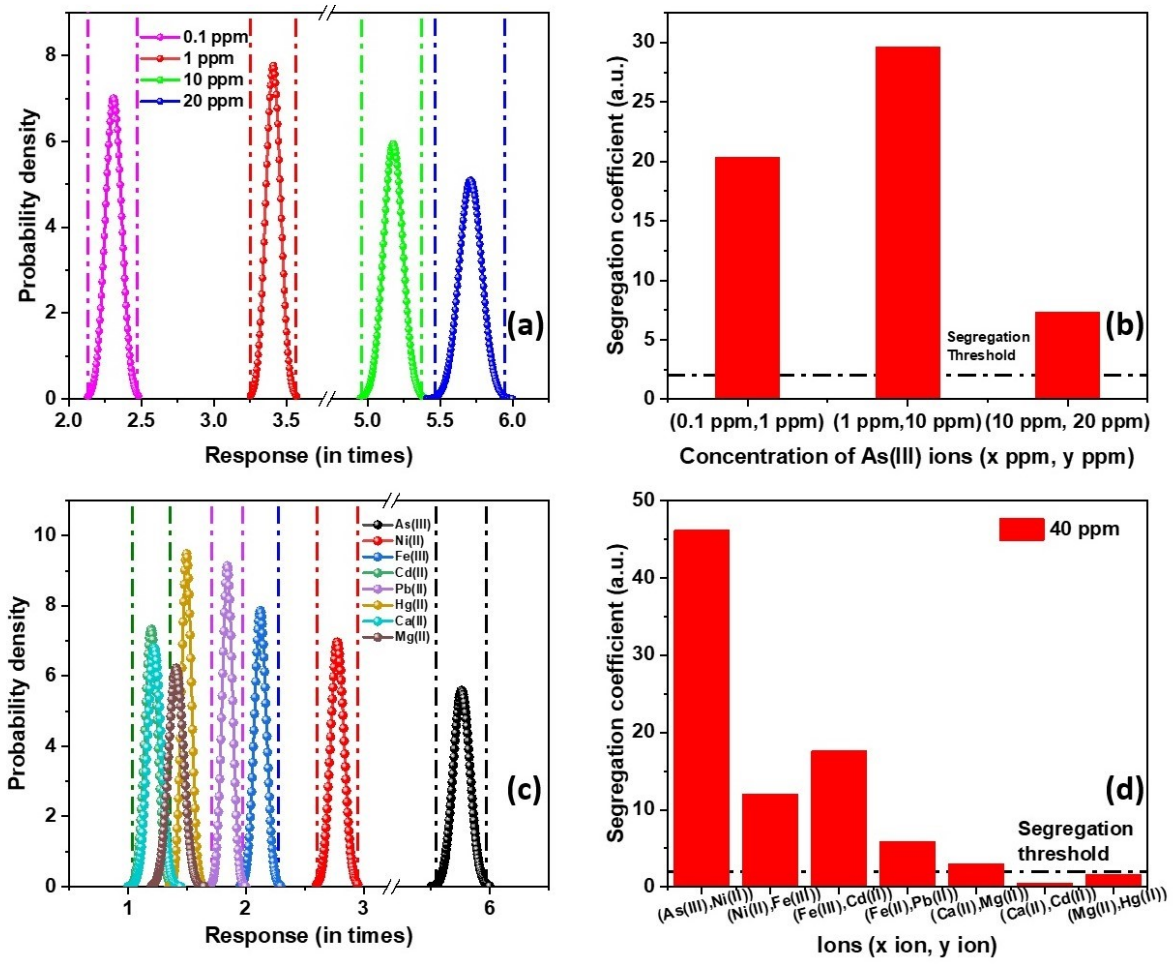

Figure S8. (a) 3-sigma separation plot for the response of device towards different concentrations of As(III) ions (b) Segregation coefficient vs concentration of As(III) ions plot showing the segregation coefficient above the segregation threshold value among the As(III) ions (c) 3-sigma separation plot for the response of device towards different heavy metal ions (d) Segregation coefficient vs different heavy metal ions plot at 40 ppm of ions showing the As(III) and Ni(II) ions segregation coefficient above the segregation threshold value

S10. Response of the sensor at various pH

Response of the sensor towards As(III) ions was tested at various pH environments (4-10). The response of the sensor was found to be almost constant across the entire pH range as shown in fig. S9 making the sensor viable for working in real-time environments.

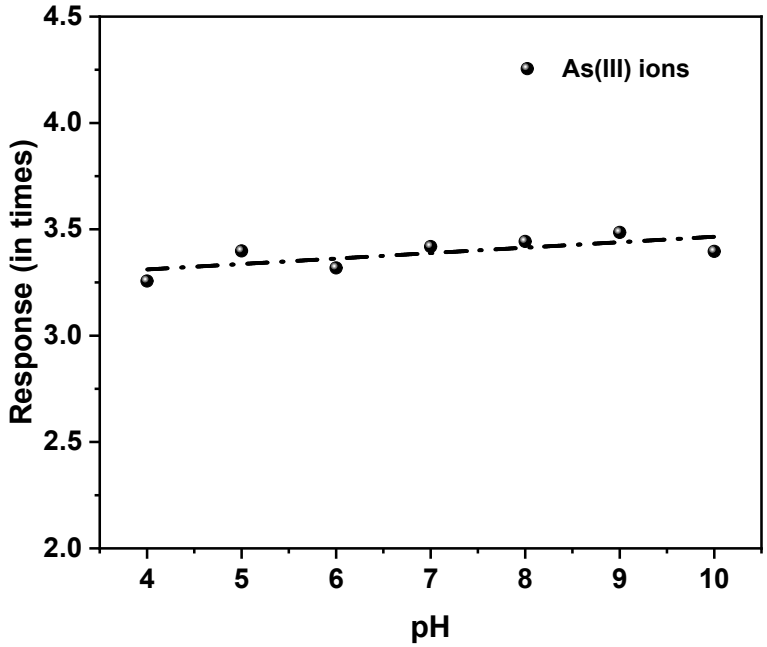

Figure S9. Variation of response of the sensor towards As(III) ions at various pH environments (4-10)

S11. Comparsion of the performance of the sensor form the literature

Table P1: Comparison table showing different As(III) ion sensors

Technique used	Sensitivity (μA/ppb)	Limit of detection (LOD)	Response time	Operating Volatge (in Volts)	System integration	Cost	Ref.
FET based	41.42	0.720 ppb	17.4 s	|0.5| (Gate bias)	Simple	Low	This work
Electrochemical	-	5.6 ppb	-	-0.5 to 0.6	Complex	Low	[1]
Electrochemical	-	5 ppb	<1 s	0.62	Complex	High	[2]
Colorimetric	-	16.9 ppb	180 s	-	Simple	Low	[3]
Surface plasmon resonance	-	10 ppb	1800 s	-	Simple	Low	[4]
Electrochemical	2.15	1.19 ppb	-	-0.2 to 0.6	Complex	Low	[5]
Electrochemical	0.85	1.51 ppb	-	-0.3 to 0.6	Complex	Medium	[6]
ICP-MS	-	10 ppb	15 mins	-	Complex	High	[7]
Electrochemical	-	0.07 ppm	-	-0.6 to 0.2	Complex	-	[8]

Table P2: Comparison table showing different field effect transistors

Channel	Gate oxide	Gate bias (volts)	Selectivity	LOD	Power Consumption	Fabrication complexity	Scalability	Ref.
rGO	GO	|0.5|	As(III) ions	0.720 ppb	In μW	Optical lithography and Drop-casting	Simple fabrication process, Low-cost device, fast (17.4 s) and found to be repeatable (tested for ten	This work

							devices)	
Graphene	GO	-1 to 1	-	-	In µW	Thin film transfer	-	[9]
Graphene	GO	>10	-	-	In µW	Electron-beam lithography and Electron-beam evaporation	Yield and reliability may improve by using Layer transfer method	[10]
N-channel depletion mode	SiO_2	1	As(III) ions	1.99 x 10^-11 M	In mW	Selective membranes	Low cost	[11]
Graphene	DNA-Gated	0.7	As(III) ions	5 x 10^-9 M	In µW	CVD	Complex fabrication process	[12]
Graphene – Tetra-phenylporphyrin	-	-	Various heavy metal ions (Cd(II), Cu(II), Fe(III), Mn(II),Ni(II))	1 x 10^-9	-	CVD and Spin-coating	Simple fabrication process and scalable owing to its one-step function-alization process	[13]
Graphene	DNA-zyme Solution gated	0.7	Pb(II) ions	0.39 ppb	In µW	Wet transfer method and Magnetron sputtering deposition	-	[14]
Graphene ion selective membrane	-	-	Cr(VI) ions	10^-6 M	-	Ion selective membrane	Testing time of sample is 10 min	[15]
MoS_2	SiO_2	>10	Hg(II) ions	0.0002 ppb	In µW	Laser optical lithography	-	[16]
ZnO@rGO	-	>0.5	Cu(II) ions	946 ppb	In mW	Screen printed Thin film	Low-cost, sensitive, reliable but LOD is high	[17]

S12. Adsorption of heavy metal ions

Adsorption of various ions (As(III), Ni(II), Pb(II) and Cd(II)) was tested using UV-Visible spectrophotometer (Ocean Insight D_2/W light source). The adsorption of As(III) ions on the receptor layer was found to be maximum as shown in fig. S10. As the concentration of As(III) ions increased, the adsorption rate increased that can be explained as the increase in adsorption sites with the increase in concentration.

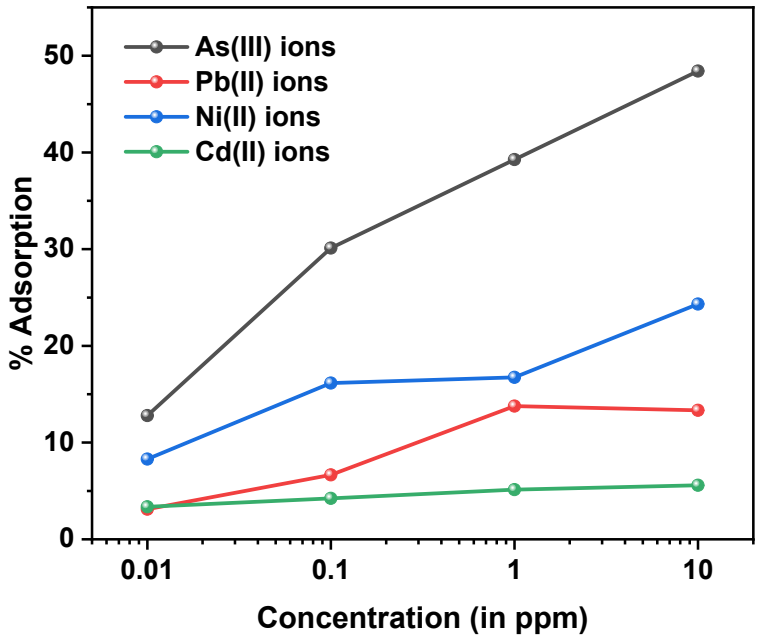

Figure S10. Variation of adsorption on the receptor surface with different concentration of various heavy metal ions (As(III), Ni(II), Pb(II) and Cd(II))

S13. Model Evaluation for Prediction of Ni(II) and As(III) ions

Table P3: Model Evaluation for Prediction of Nickel Concentration Using Original Current Feature

Model	R^2 Score	Correlation (r)
Linear Regression	0.9732	0.9826
Lasso Regression	0.1181	0.4776
Ridge Regression	0.1771	0.5245
Random Forest	0.6238	0.8185
Gradient Boosting	0.4992	0.7081
AdaBoost	0.4753	0.7486
XGBoost	0.3657	0.6141
CatBoost	0.5519	0.7652
SVR	-0.0299	0.3062
KNN Regressor	0.2504	0.5120
Decision Tree	0.4806	0.7279

Table P4: Model Evaluation for Prediction of Nickel Concentration Using Original Current Feature

Model	R^2 Score	Correlation (r)
Linear Regression	0.9812	0.9841
Lasso Regression	-0.0241	0.0119
Ridge Regression	-0.0093	0.1007
Random Forest	0.4131	0.6448
Gradient Boosting	0.3633	0.6152
AdaBoost	0.2840	0.5426
XGBoost	0.5134	0.7341
CatBoost	0.2217	0.5163
SVR	0.1817	0.4832
KNN Regressor	0.1569	0.4793
Decision Tree	-0.2142	0.4479

S14. Dielectric constant of Graphene oxide (GO)

The dielectric constant of GO was found using impedance spectroscopy. The dielectric constant of GO was found to be around 860 as shown in fig. S11 below**.**

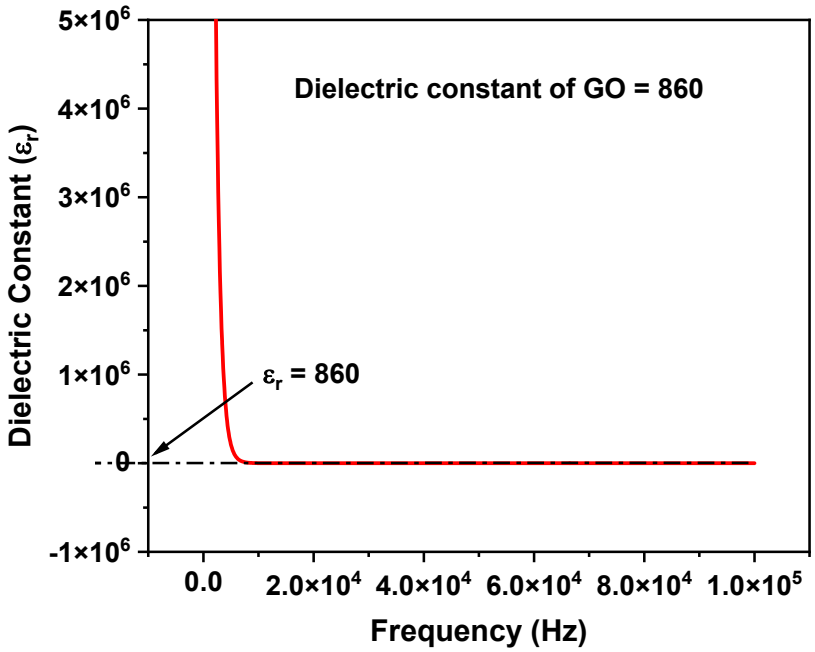

Figure S11. Plot of Dielectric constant variation of GO with increase in frequency

S15. Derivation for As(III) Sensing mechanism

The drain current in the FET in the saturation region is given by:

$$I_D = \frac{\mu_p C_{ox} W}{2L}(V_{GS} - V_{th})^2 \qquad (1)$$

where I_D is the drain current that is flowing through the semiconductor, μ_p is the mobility of the holes having a value of 800 cm^2/Vs , C_{ox} is the oxide capacitance, W is the width of the channel and L is the length of the channel, V_{GS} is the gate to source voltage applied, V_{th} is the threshold voltage of the FET and V_{DS} is the voltage applied across the drain of the FET.

In the above equation (1), replacing C_{ox} by $C_{ox} = \frac{k \in_o A}{d}$ we get,

$$I_D = \frac{\mu_p k \in_o AW}{2Ld}(V_{GS} - V_{th})^2 \qquad (2)$$

where 'k' is the dielectric constant, 'A' is the cross-sectional area and 'd' is the oxide thickness.

From here, replacing A with A= WL where W is the length of the electrode which is the width of the channel and L is length of the channel which is the distance between the electrodes,

$$I_D = \frac{\mu_p k \in_o .WL.W}{2Ld}(V_{GS} - V_{th})^2 \qquad (3)$$

which can be rewritten as:

$$I_D = \frac{\mu_p k \in_o .W^2}{2d}(V_{GS} - V_{th})^2 \qquad (4)$$

Now, the change in current with respect to time is given by :-

$$dI(t) = \frac{Q}{t} = C\frac{dV}{dt} \qquad (5)$$

where Q is the charge and t is the time.

Now, combining the above equation (4) and (5), equation (6) is obtained that is

$$\frac{dI(t)}{I_{bare}}dt = \alpha\frac{dV}{(V_{GS} - V_{th})^2} \qquad (6)$$

where α is a constant with a value of 1.875 cm^4/Vs.

Integrating both sides, equation (8) is obtained (As mentioned in the main manuscript section **3.3 Mechanism of As(III) ion sensing**).

S16. Hysteresis curve of rGO/GO FET based As(III) Sensor

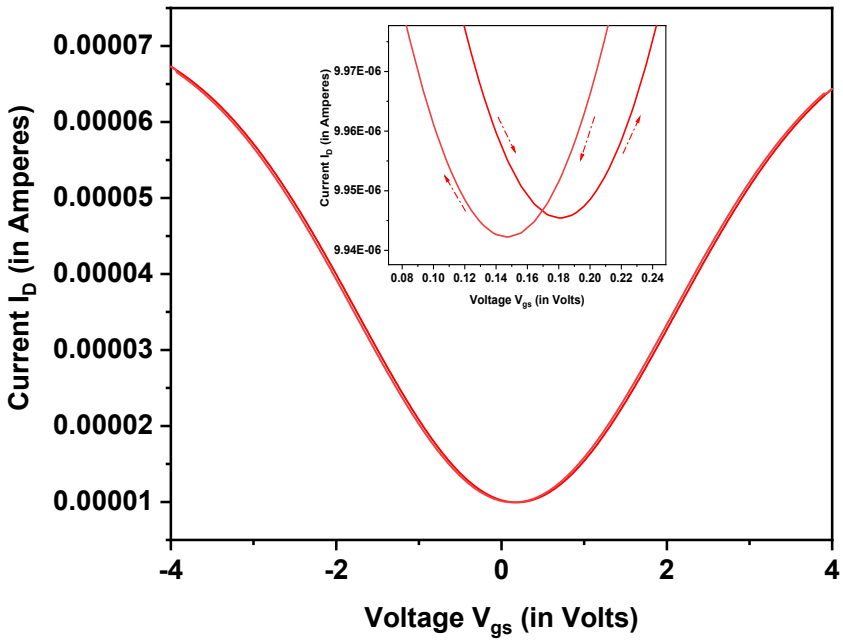

Figure S12. Hysteresis curve of rGO/GO FET for a V_{DS} of 0.5 V

Hysteresis test of the rGO/GO FET is performed. The FET exhibits a Dirac shift of around 35 mV showing the stability of the heavy metal ion FET based sensor as shown in fig. S12.

References

[1] Ismail, Suhainie, Nor Azah Yusof, Jaafar Abdullah, and Siti Fatimah Abd Rahman. “Development of electrochemical sensor based on silica/gold nanoparticles modified electrode for detection of arsenite.” IEEE Sensors Journal 20, no. 7 (2019): 3406-3414.

[2] Bhanjana, Gaurav, Neeraj Dilbaghi, Savita Chaudhary, Ki-Hyun Kim, and Sandeep Kumar. “Robust and direct electrochemical sensing of arsenic using zirconia nanocubes.” Analyst 141, no. 13 (2016): 4211-4218.

[3] Nguyen, Nguyen Le Thao, Chan Yeong Park, Jong Pil Park, Suresh Kumar Kailasa, and Tae Jung Park. Synergistic molecular assembly of an aptamer and surfactant on gold nanoparticles for the colorimetric detection of trace levels of As 3+ ions in real samples. New Journal of Chemistry 42, no. 14 (2018): 11530-11538.

[4] Solanki, Pratima R., Nirmal Prabhakar, Manoj K. Pandey, and Bansi D. Malhotra. “Surface plasmon resonance-based DNA biosensor for arsenic trioxide detection. International Journal of Environmental and Analytical Chemistry 89, no. 1 (2009): 49-57.

[5] Hu, Haibing, Wenjie Lu, Xingnan Liu, Fancheng Meng, and Jianxiong Zhu. "A high-response electrochemical As (III) sensor using Fe3O4–rGO nanocomposite materials." *Chemosensors* 9, no. 6 (2021): 150.

[6] Radinović, Kristina, Jadranka Milikić, Nemanja Gavrilov, Dalibor Stanković, Aleyna Basak, Önder Metin, and Biljana Šljukić. "Analytical performance and stability studies of CoAu/rGO-based electrochemical sensor for arsenic (III) detection in aqueous solutions." *Talanta* (2025): 128305.

[7] Stetson, Sarah J., Caitlyn Lawrence, Susan Whitcomb, and Christopher Kanagy. "Determination of four arsenic species in environmental water samples by liquid chromatography-inductively coupled plasma-tandem mass spectrometry." *MethodsX* 8 (2021): 101183.

[8] Zhao, Ke, Canwei Mao, Ruiyu Ding, Dean Song, Liya Ge, and Grzegorz Lisak. "Simultaneous speciation of inorganic arsenic (III and V) utilizing gold-manganese oxide nanoparticles modified electrochemical sensors." *Electrochimica Acta* 502 (2024): 144796.

[9] Lee, Seoung-Ki, Ho Young Jang, Sukjae Jang, Euiyoung Choi, Byung Hee Hong, Jaichan Lee, Sungho Park, and Jong-Hyun Ahn. All graphene-based thin film transistors on flexible plastic substrates. Nano letters 12, no. 7 (2012): 3472-3476.

[10] Standley, Brian, Anthony Mendez, Emma Schmidgall, and Marc Bockrath. Graphene–graphite oxide field-effect transistors. Nano Letters 12, no. 3 (2012): 1165-1169.

[11] Tatavarthi, Sai Sudheer, Shin-Li Wang, Yu-Lin Wang, and Jung-Chih Chen. "Rapid and highly sensitive extended gate FET-based sensors for arsenite detection using a handheld device." *ECS Journal of Solid State Science and Technology* 9, no. 11 (2020): 115014

[12] Wang, Yuhong, Yulong Bi, Rongrong Wang, Lu Wang, Hao Qu, and Lei Zheng. "DNA-gated graphene field-effect transistors for specific detection of arsenic (III) in rice." *Journal of Agricultural and Food Chemistry* 69, no. 4 (2021): 1398-1404.

[13] Tuerdi, Gulimire, Qinqiang Zhang, Lei Bao, Xiaoyan Zhang, Ken Suzuki, Hideo Miura, Zhengjun Zhang, and Wangyang Fu. "Highly Sensitive Metal Ion Detection Using Tetraphenylporphyrin-Functionalized Graphene Field-Effect Transistors." *ACS Applied Electronic Materials* (2025).

[14] Zhao, Siyu, Jing Yang, Lu Wang, Baolei Dong, Yu Mao, Hao Qu, and Lei Zheng. "Selective detection of Pb2+ ions based on a graphene field-effect transistor gated by DNAzymes in binding mode." *Biosensors and Bioelectronics* 237 (2023): 115549.

[15] Liu, Tzu-Yu, Huai-Yuan Hsu, Huan-Cheng Liu, and Nien-Tsu Huang. "Continuous and automatic hexavalent chromium sensing using an ion-selective membrane deposited ion-sensitive field-effect transistor device integrating a microfluidic control system." *Lab on a Chip* (2025).

[16] Urbanos, Fernando J., Sara Gullace, and Paolo Samorì. Field-effect-transistor-based ion sensors: ultrasensitive mercury (II) detection via healing MoS2 defects. Nanoscale 13, no. 46 (2021): 19682-19689.

[17] Kim, Eun-Bi, M. Imran, Eun-Hee Lee, M. Shaheer Akhtar, and Sadia Ameen. Multiple ions detection by field-effect transistor sensors based on ZnO@ GO and ZnO@ rGO nanomaterials: Application to trace detection of Cr (III) and Cu (II). Chemosphere 286 (2022): 131695.